Since January 2020 Elsevier has created a COVID-19 resource centre with free information in English and Mandarin on the novel coronavirus COVID-19. The COVID-19 resource centre is hosted on Elsevier Connect, the company's public news and information website.

Science of the Total Environment 655 (2019) 787–795

Contents lists available at ScienceDirect

Science of the Total Environment

journal homepage: www.elsevier.com/locate/scitotenv

Inactivation of airborne bacteria using different UV sources: Performance modeling, energy utilization, and endotoxin degradation

Can Wang *, Siyi Lu, Zhiwei Zhang

School of Environmental Science and Engineering, Tianjin University, Tianjin 300350, PR China
Tianjin Key Lab of Indoor Air Environmental Quality Control, Tianjin 300350, PR China

HIGHLIGHTS

- UV inactivation performance was simulated by a Beer-Lambert law-based model.
- The inactivation efficiency of three UV sources was compared.
- Low influent *E. coli* concentrations and high UV doses resulted in high EC value.
- The release and removal of free and bound endotoxins were observed.

GRAPHICAL ABSTRACT

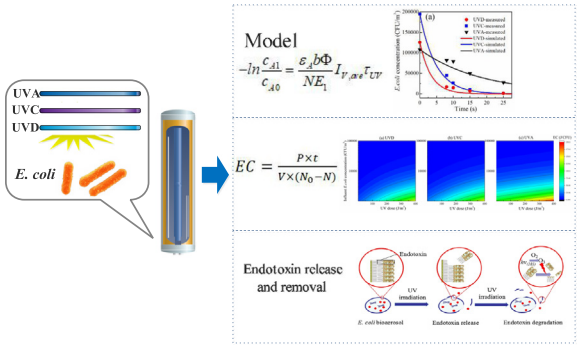

ARTICLE INFO

Article history:
Received 30 July 2018
Received in revised form 23 October 2018
Accepted 17 November 2018
Available online 20 November 2018

Editor: Ching-Hua Huang

Keywords:
Bioaerosol
UV germicidal irradiation (UVGI)
Model
Energy utilization
Airborne endotoxin

ABSTRACT

Airborne bacteria-containing bioaerosols have attracted increased research attention on account of their adverse effects on human health. Ultraviolet germicidal irradiation (UVGI) is an effective method to inactivate airborne microorganisms. The present study models and compares the inactivation performance of three UV sources in the UVGI for aerosolized *Escherichia coli*. Inactivation efficiency of 0.5, 2.2 and 3.1 logarithmic order was obtained at an exposure UV dose of 370 J/m^3 under UVA (365 nm), UVC (254 nm) and UVD (185 nm) sources, respectively. A Beer–Lambert law-based model was developed and validated to compare the inactivation performances of the UV sources, and modeling enabled prediction of inactivation efficiency and analysis of the sensitivity of several parameters. Low influent *E. coli* concentrations and high UV doses resulted in high energy consumption (EC). The change in airborne endotoxin concentration during UV inactivation was analyzed, and UVC and UVA irradiation showed no marked effect on endotoxin degradation. By contrast, both free and bound endotoxins could be removed by UVD treatment, which is attributed to the ozone generated by the UVD source. The results of this study can provide a better understanding of the air disinfection and airborne endotoxin removal processes.

1. Introduction

Bioaerosols are airborne microbial cells with fragments and particulate matter of biological origin (Liang et al., 2012). These small particles affect human health by causing infectious diseases, acute toxic reactions, and allergies (Gergen, 2011). Prevention and control measures for bioaerosols have attracted worldwide attention as a result of the

* Corresponding author at: School of Environmental Science and Engineering, Tianjin University, Tianjin 300350, PR China.
E-mail address: wangcan@tju.edu.cn (C. Wang).

https://doi.org/10.1016/j.scitotenv.2018.11.266
0048-9697/

recent pandemics of severe acute respiratory syndrome (SARS) and influenza H1N1 (Zhang et al., 2010). Ultraviolet germicidal irradiation (UVGI) systems are used as commercial engineering controls to prevent the transmission of infectious diseases (Jensen et al., 1994). UVGI is an effective method of inactivating airborne microorganisms (Xu et al., 2005). Germicidal lamps containing mercury vapors under low pressure are a commonly used UV source for UVGI (Ryan et al., 2010).

Microorganisms present different UV sensitivities, which is often measured by the UV fluence required for decreasing one logarithmic order of bacterial number (Lytle and Sagripanti, 2005; Sagripanti et al., 2009), and this value of 70.3, 73.3, and 18.3 $J \cdot m^{-2}$ have been observed for vegetative cells of *B. atrophaeus*, *P. agglomerans*, and *Y. ruckeri*, respectively (King et al., 2011). Higher UV sensitivity was observed at higher relative humidity according to Walker's study on MS2 Bacteriophage (Walker and Ko, 2007). Other than the species of microorganism and relative humidity (Xu et al., 2005), UV wavelength is also an important parameter determining the UV inactivation efficiency of bacterial aerosol. Maximum effectiveness is usually observed at around 254 nm (UVC) (Koller, 1952) and many studies have been conducted on the inactivation of airborne microorganisms by using UVC radiation. Inactivation performance under other UV wavelengths has also been explored. Kim and Jang (2018), for example, investigated several photocatalytic reactions by UVD (185 nm) with short irradiation times to inactivate airborne MS2 viruses. Araud et al. (Araud et al., 2018) also investigated the inactivation mechanisms of viruses via solar UVA and visible light. However, the inactivation performance of different UV sources, especially UVD, which can damage microorganisms by producing ozone in addition to UV irradiation, has rarely been compared. In addition, few studies have reported the energy efficiency of UVGI devices, which is also a factor to consider when choosing a UV source with which to conduct inactivation.

The effectiveness of UVGI devices has been modeled in previous studies, as summarized in Table 1. Inactivation kinetics has been being studied since twentieth century (Crittenden et al., 2011). Reaction rates vary by one and one-half orders of magnitude for UV disinfection (Zhao et al., 2014). Utilization of the Chick-Watson model (Ryan et al., 2010; Xu et al., 2003; Kowalski and William, 2000) is the standard method for modeling the response of microorganisms to UVGI. In some cases, the two-stage curve (Noakes et al., 2015), such as Rennecker-Marinasis model (Crittenden et al., 2011) and Collins-Selleck model (Collins and Selleck, 1971), were used to describe the unusually high resistance of microorganisms to irradiation because many microbial decay curves exhibit a decay curve shoulder (time-delayed response) when exposed to UVGI. Most of the previous models were kinetic fitting of inactivation efficiency, while the present work takes mechanism of photoreaction into account, providing more insight into the process of UV inactivating bacteria.

Microbial inactivation through UVGI results from denaturation of enzymes, proteins, and membranes and disruption of cellular metabolic activities (Takashima et al., 2007). However, intracellular substances may be released when the cells in bioaerosols are damaged or destroyed (Mattsbybaltzer et al., 1991). Endotoxins are complexes of lipopolysaccharides (LPS), proteins, and hazardous biological substances (Fig. S1 in Supporting Information) (Liu et al., 2018; Wen et al., 2017). They are widely distributed in the outer cell wall membranes of Gram-negative bacteria and other microorganisms (Nilsson et al., 2011).

Several studies have observed waterborne endotoxin release during inactivation of Gram-negative bacteria (Dufour et al., 2017; Zhang et al., 2016; Sreeja and Shetty, 2016). The results of these works verify that embedded endotoxins can be released into the environment after the death of bacteria or cells. Airborne endotoxins may exist as shed membrane complexes (free endotoxins) or bound endotoxins when combined with other biological and nonbiological particles (Oldenburg et al., 2007). Chronic exposure to endotoxins induces and exacerbates airway symptoms (Mendy et al., 2016), such as asthma, coughing, chronic obstructive pulmonary diseases, and organic dust lung diseases (Kong et al., 2013; Reiman and Uitti, 2000). Endotoxins released from airborne bacteria under UV irradiation have not been reported.

In this study, the inactivation performances of three different UV sources toward aerosolized *Escherichia coli* (*E. coli*) were investigated and compared, and the inactivation efficiency and rate of these sources were analyzed. A Beer–Lambert law-based model was developed and validated to compare the inactivation performances of the UV sources, and their of energy utilization efficiencies during UV irradiation were analyzed. The distribution and fate of airborne endotoxins were also investigated. The results of this study may provide important insights into the control of airborne microbes by using UV irradiation and help mitigate the environmental impacts of bioaerosols.

2. Materials and methods

2.1. Preparation and generation of airborne E. coli

E. coli (CMCC1.3373) inoculated into nutrient broth medium was cultured in a constant-temperature oscillation incubator (IS-RSDA, Crystal Technology & Industries, Inc., USA) at 37 °C and 170 r/min for 24 h. The suspension was centrifuged at 4000 r/min for 10 min, washed thrice with 0.85% NaCl solution to remove the medium, and then diluted. The bacteria-containing aqueous suspension was aerosolized by

Table 1
Summary of models on bacteria inactivation using UV irradiation.

Model	Equation	Reference
Chick-Watson	$\ln(\frac{N}{N_0}) = -kIt$ where I = UV intensity, W/m^2 t = exposure time, s k = inactivation rate, m^2/J.	Ryan et al., 2010
Scheible	$N(t) = {N_0}^{-kD} + \frac{N_0}{kD}(1-e^{-kD})$ where D = UV dose, J/m^2 k = inactivation rate constant, s^{-1}.	Gibson et al., 2017
Rennecker-Marinas	For $It < b$, $\ln(\frac{N}{N_0}) = 0$ For $It > b$, $\ln(\frac{N}{N_0}) = \Lambda_{CW}(b-Ct)$ where $\hat{}_{cw}$ = coefficient of specific lethality, $1/(J/m^2)$, b = lag coefficient, J/m^2.	Crittenden et al., 2011
Collins-Selleck	For $It < b$, $\ln(\frac{N}{N_0}) = 0$ For $It > b$, $\ln(\frac{N}{N_0}) = \Lambda_{CW}[(\ln(b)-Ct)]$ where $\hat{}_{cw}$ = log-based coefficient of specific lethality, $1/(J/m^2)$, b = lag coefficient, J/m^2.	Collins and Selleck, 1971

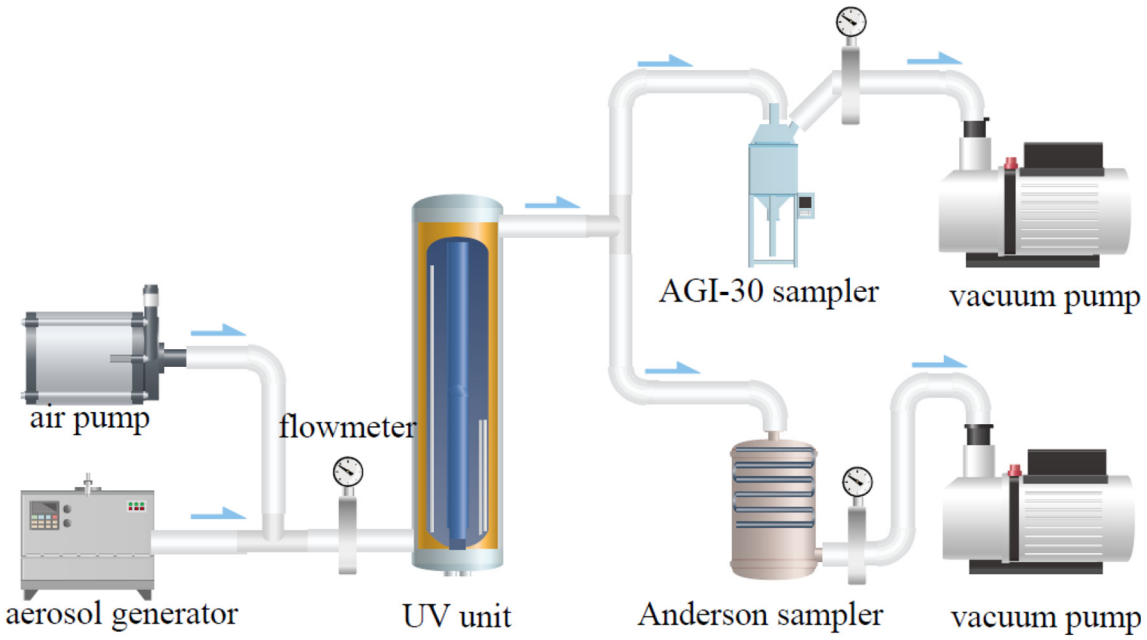

Fig. 1. Experimental setup for bioaerosol exposure to the UVGI.

an aerosol generator (Topas, ATM226, Germany) to particle size of 1–5 μm (Fig. S2 in Support Information).

2.2. Experimental set-up for UVGI system

A schematic representation of the experimental setup for inactivating airborne microorganisms is shown in Fig.1. The UV unit is cylinder-shaped with its dimension of Φ7cm × 47 cm, including a vertically placed ultraviolet lamp in it. UV irradiation of UVA (365 nm), UVC (254 nm) and UVD (185 nm) was obtained using three kind of commercial low pressure mercury lamp with two types of output power (GPH550T5L, 28W and GPH287T5L, 14W, Hanovia Ltd., USA). The bacterial bioaerosol is generated by nebulizing the bacteria-containing aqueous suspension, diluted with sterile air. The air stream containing airborne bacteria passed through UV unit from bottom to top, and was subsequently collected and measured.

The airflow rate varied through the UV unit to change the bacteria's exposure time to UV irradiation, ranging from 0.26 to 0.65 m^3/h. UV dose is obtained by multiplying $I_{v,ave}$ by exposure time, where $I_{v,ave}$ is calculated using LSSE model as discussed before, and exposure time is determined by the reactor volume(m^3) divided by airflow rate (m^3/h). The bacteria concentration was calculated as CFUs obtained by plate counting method divided by the volume of collected bioaerosol (m^3). Besides, each of experiments was conducted in duplication.

Table 2
Summary of models on determination of the average absorbed energy density inside various reactors.

Model	Reactor type	Reaction phase	Abstract	Classification	Reference
Two-fluid model	Cube	Liquid-gas	Prediction of energy flow density	Incidence model	Akehata et al., 1976
	Tube	Bubbling dispersion system, Gas-solid-liquid phase	Prediction of energy flow density	Radial incidence model	Inokawa, 1980
Model based on distribution function	Tube	Air phase	Estimation of absorption rate of radiation energy	Incidence model	Yokota et al., 1981
		Water or NIS solution system	Estimation of filter effect of dispersed phase	Incidence model	
	Tubular bubble tower	Nitrogen radiation measurement system	Estimation of absorption rate of radiation energy on account of air/water ratio	LSDE	Yokota et al., 1981
		Nitrogen-chorine-toluene system	Estimation of radiation energy absorption rate in half-batch reactor	LSDE	Yokota et al., 1981
Model based on Monte-carlo method	Tube	Absorption-diffusion medium	Estimation of energy absorption in a continuous reactor	LSSE	Jacob and Dranoff, 1968
	Parallel plate	Fiber bundle suspension system	Prediction of the absorption rate of light energy in light synthesis reaction, on account of cell concentration	Point lights model	Koizumi et al., 1980
Model based on effective absorption rate	Cubic bubble tower	Nitrogen-potassium nitrate aqueous solution	Estimation of radiation field in gas-liquid dispersed phase	LSPP, LSDE	Otake et al., 1983
	Tubular bubbling tower	Nitrogen-aqueous solution	Estimating the absorption rate of Light Energy in Gas-liquid system on account of modified attenuation coefficient	LSDE	Yokota et al., 1981
	Annular stirring tower	Chlorine-nitrogen-chloroform solution	Prediction of the energy absorption rate of chlorination Reaction	ESVE	Alfano et al., 1986

LSDE: Line Source Diffuse Emission; LSSE: Line Source Spherical Emission.
LSPP: Line Source Parallel Plane; ESVE: Extense Source Volumetric Emission.

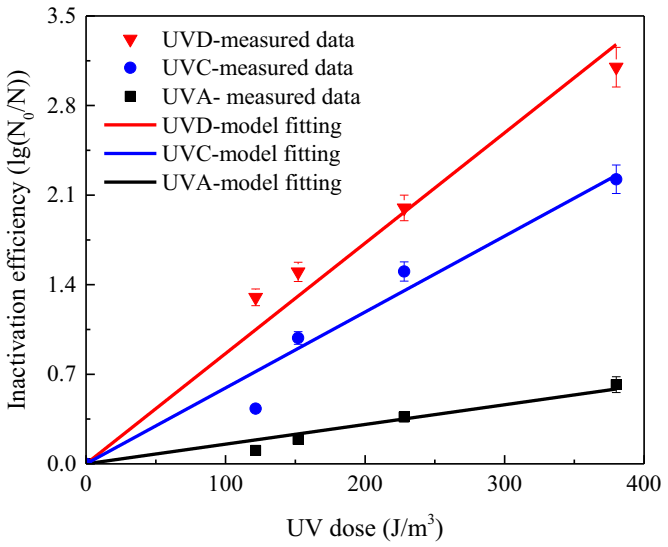

Fig. 2. Model fitting of airborne *E.coli* inactivation under different UV sources (UV density = 15.2 W/m^3).

2.3. Sampling and analysis of airborne E. coli

A six-stage Andersen sampler (ZLKZR-B01, Beijing Jolyc Technology Co., Ltd., China) was used to obtain bioaerosol samples. A glass Petri dish containing 25 mL of nutrient agar medium was placed on each stage of the device, and samples were obtained at a flow rate of 28.3 L/min for 5 min. After sampling, the nutrient agar plates were incubated for 48 h in a constant-temperature incubator at 37 °C. The number of colony-forming units (CFUs) on each nutrient agar plate was manually counted.

2.4. Airborne endotoxin analysis

Airborne endotoxin samples (Liu et al., 2018) were collected with an AGI-30 impinger (Qingdao Junray Intelligent Instrument Co., Ltd., China). Samples were stored in a sealed pyrogen-free flask at 4 °C for no more than 2 h. The airborne endotoxin concentrations of the samples were determined using a limulus amebocyte lysate (LAL) assay reagent with a chromogenic endpoint. The kinetic chromogenic LAL assay is widely applied to airborne endotoxin tests (Liu et al., 2018; Wen et al., 2017).

Airborne endotoxins may exist in a bound or free state (Demonty and Grawe, 1982). Bound endotoxins remain bound to the bacterial outer membrane, whereas free endotoxins are shed from membrane complexes containing phospholipids, proteins, and LPS. Water samples were filtered through a 0.22 μm PTFE membrane prior to the LAL assay. The endotoxin that remained in the filtrate was referred to as "free-endotoxin". The amount of endotoxin determined prior to filtration was referred to as "total-endotoxin". The amount of "bound-endotoxin" was measured by subtracting the "free-endotoxin" from the "total-endotoxin". A schematic of LAL method and detailed information on the detection of airborne endotoxins is provided in Fig. S3 in the Supporting Information.

Table 3
Model fitting results.

UV source	Reaction rate constant k (s^{-1})	Fitting formula	R^2
UVD	0.131	$\lg\frac{N_0}{N} = 0.00862 I_{UV}\tau_{UV}$	0.9925
UVC	0.090	$\lg\frac{N_0}{N} = 0.00593 I_{UV}\tau_{UV}$	0.9863
UVA	0.023	$\lg\frac{N_0}{N} = 0.00154 I_{UV}\tau_{UV}$	0.9822

$\lg\frac{N_0}{N_{UV}} = kt$, where inactivation rate constant k (s^{-1}) was defined as the log order of bacteria number being inactivated per unit time.

2.5. Modeling of airborne E. coli inactivation by UV irradiation

2.5.1. Photochemical process

In the gas phase, photons are absorbed to inactivate bacteria in bioaerosols. Herein, the quantum yield (Φ) is defined as follows:

$$\Phi = \frac{dN_A}{dx} \tag{1}$$

where N_A is the number of inactivated airborne bacteria and x is the number of absorbed photons.

The equation can be further expanded as follows:

$$-\frac{dc_A}{dt} = \frac{\Phi}{NE_1} I_V \tag{2}$$

where c_A is the concentration of airborne bacteria, N (mol^{-1}) is the Avogadro constant of 6.023×10^{23} (Becker, 2001), E_1 (J) is the energy of one photon, I_V ($W \cdot m^{-3}$) is the absorbed energy density, and t (s) is the exposure time.

Based on the Beer–Lambert law (Mortensen and Xiao, 2007), the kinetic model for bacterial inactivation can be written as follows:

$$I = I_0\left(1 - e^{\varepsilon_A C_A b}\right) \tag{3}$$

where ε_A ($dm^3 \cdot mol^{-1} \cdot cm^{-1}$) is the molar extinction coefficient, b (cm) is the optical length, and I and I_0 ($W \cdot m^{-3}$) are the absorbed and incident energy densities, respectively.

From Eqs. (2) and (3),

$$-\frac{dc_A}{dt} = \frac{\Phi}{NE_1} I_{V,0}\left(1 - e^{-\varepsilon_A c_A b}\right) \tag{4}$$

UV light absorption is a weak process in the gas phase; hence,

$$1 - e^{-\varepsilon_A c_A b} \approx \varepsilon_A c_A b \tag{5}$$

Therefore,

$$-\frac{dc_A}{dt} = -r_A = \frac{\Phi}{NE_1} I_{V,0} \varepsilon_A c_A b \tag{6}$$

where $-r_A$ ($mg \cdot m^{-3} \cdot hr^{-1}$) is the bacterial inactivation rate.

2.5.2. Photochemical inactivation in the UV reactor

The flow pattern of the UV reactor used in this study can be considered as an ideal plug flow. Thus, the following equation is given as follows:

$$\frac{dc_A}{dt} = -\frac{d(Q\ c_A)}{dV} \tag{7}$$

where Q ($m^3 \cdot h^{-1}$) is the gas flow rate, V (m^3) is the reactor volume, and t (sec) is the time. From Eqs. (6) and (7):

$$-\ln\frac{N_{UV}}{N_0} = \frac{\varepsilon_A b \Phi}{NE_1} I_{V,ave} \tau_{UV} \tag{8}$$

where N_{UV} and N_0 are the respective bacterial concentrations in the bioaerosol at the outlet and inlet (CFU/m^3), $I_{V,\ ave}$ ($W \cdot m^{-3}$) is the average absorbed energy density inside the reactor. τ (sec) is exposure time inside the reactor, which is calculated as reactor volume(m^3) divided by airflow rate (m^3/s).

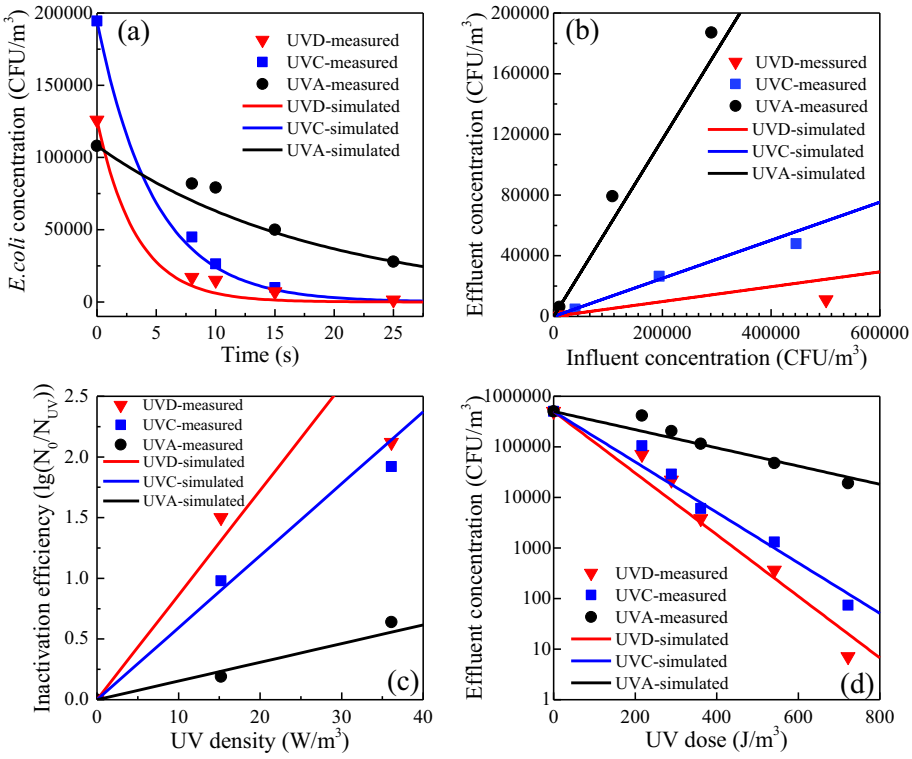

Fig. 3. Model simulation and verification in terms of (a) retention time (b) influent *E.coli* concentration (c) UV average absorbed energy density (d) UV dose.

2.5.3. Determination of the average absorbed energy density

The average absorbed energy density inside the reactor was calculated by the line source with spherical emission (LSSE) model. A summary of models and detailed information for solving $I_{V,ave}$ can be found in Table 2 and Fig. S4 in the Supporting Information.

$$I_{ave,\lambda} = \frac{S_L P_{i,\lambda}}{2V} \int_0^H \cdot \int_{r_1}^R \cdot \int_0^L \frac{\exp\left(-\mu_i (r-r_1)\sqrt{r^2+(z-l)^2}/r\right)}{r^2+(z-l)^2} rdldrdz \tag{9}$$

where S_L ($W \cdot m^{-1}$) is the light source strength per unit length (lamp power divided by lamp length), λ (nm) is the wavelength, P_i is the emitting energy fraction at wavelength λ_i, V is the reactor volume, H is the reactor height, r_1 is the lamp radius, R is the reactor internal radius, L is the lamp length, μ_i is the absorbency per unit optical thickness, r (m) is the radial coordinate, z (m) is the rectangular coordinate, and l (m) is the point source height.

Using the LSSE model, the UV average absorbed energy densities of two lamps in this study (with different powers and lengths) were calculated to be 15.2 and 36.1 W/m^3, respectively.

3. Results and discussion

3.1. Model fitting and simulation of inactivation performance by UVGI

3.1.1. Model fitting

The experimental data obtained from the three UV sources with a UV average absorbed energy density of 15.2 W/m^3 were fitted to a model to obtain the related parameters. The inactivation efficiency (E) is defined as the logarithmic order of bacteria concentration decreasing after UV inactivation (Ishiguro et al., 2013; Wang et al., 2018):

$$E = \lg \frac{N_0}{N_{UV}} \tag{10}$$

As shown in Fig. 2 and Table 3, inactivation efficiency showed pseudo-first-order reaction kinetics, which also indicates that it corresponds to the theoretical model where the inactivation rate constant k (s^{-1}) under the three UV sources is related to ε_A, b, and Φ.

In Fig. 2, the inactivation efficiency of the three UV sources gradually increased at different rates with increasing exposure time or UV dose. The inactivation rate increased under different UV wavelengths, following the order UVD > UVC > UVA at the same exposure time. The UV doses required to decrease 1 logarithmic (lg) order of airborne *E. coli* by UVD, UVC, and UVA irradiation were 116, 169, and 649 J/m^3, respectively. At an exposure UV dose of 370 J/m^3, the inactivation efficiency of UVD was 3.1 lg orders, which is slightly higher than that of UVC, which was 2.2 lg orders. The inactivation efficiency of UVA was much lower than those of the two other UV irradiation sources, and its efficiency was only 0.5 lg orders at the same UV dose.

The effective performance of UVD could be attributed to the generation of reactive oxygen species (Ono et al., 2016) by vacuum ultraviolet photolysis of water vapor. UVC irradiation is generally utilized to inactivate aerosolized microorganisms because bacterial cells strongly absorb UV radiation (peak absorption, 250–270 nm). The generally accepted mechanism for this process is that UV irradiation inactivates bacteria by damaging their DNA, thereby preventing microorganisms from replicating and multiplying. While the damage to DNA molecules brought about by UVA irradiation (Tang and Guo, 2005) is far less than that brought about by UVC, UVA still confers slight damage to the B-form backbone of bacterial DNA by cutting off phosphodiester bonds and disrupting the main spatial structure of DNA as well as affecting the thymine groups.

Table 4
RSI of main operating parameters.

Parameter	c_{A0}	τ	S_L	r	Q
RSI	1	−1.703	−1.703	−1.767	2.072

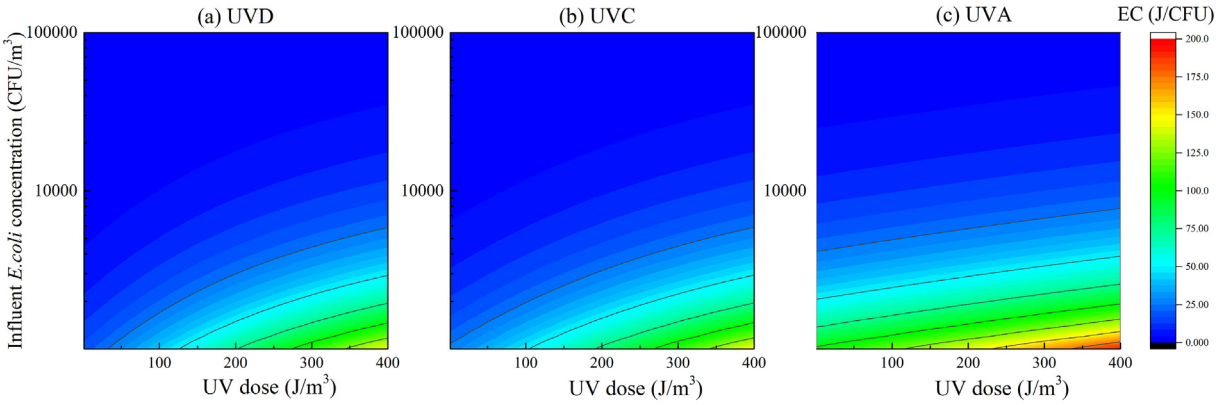

Fig. 4. EC calculation under (a) UVD (b) UVC (c) UVA source.

3.1.2. Model stimulation of inactivation performance by UVGI

Experimental data on inactivation efficiency were obtained under two UV average absorbed energy densities (15.2 and 36.1 W/m^3). The linear relation of inactivation efficiency versus UV dose was fitted according to the former set of data obtained at 15.2 W/m^3, and the inactivation rate constant k obtained in this step was used to predict the relation under the latter UV average absorbed energy density condition (36.1 W/m^3). Results are shown in Fig. 3.

Fig. 3(a)–(d) illustrate the effects of exposure time, initial bacteria concentration, UV average absorbed energy density, and UV dose on effluent bacteria concentration, which are four key parameters for reactor design and performance. Given a certain influent bacteria concentration, the curve of predicted effluent concentration after exposure to the three UV sources based on the inactivation rate constant k (Fig. 2) is shown in Fig. 3(a); measured values are also marked individually.

Comparison of the predicted and measured values reveals that the model is reasonable. Experiments on three influent bacteria concentrations (generated by nebulizing bacterial suspensions of 10^6, 10^7, and 10^8 CFU/mL) and two UV average absorbed energy densities were conducted to explore their influence on k. The prediction results of the curve in Eq. (9) and the values measured at an exposure time of 10 s are shown in Fig. 3(b) and (c). Straight lines with different slopes indicate that the influent concentration and UV average absorbed energy density have no effect on k, which coincides with the model. This finding confirms that inactivation efficiency remains relatively unchanged despite variations in initial bacteria concentration but increases with increasing UV average absorbed energy density.

3.2. Parameter sensitivity of model

To evaluate the sensitivity of the objective function to changes in different parameters in the model, the relative sensitive index (RSI) is defined as follows:

$$RSI = \frac{(y_i - y_{i0})}{(p - p_0)} \frac{p_0}{y_{i0}} \tag{11}$$

where p_0 and p are the values of an operating parameter before and after adjustment, respectively, y_{i0} is the original value of the objective function, and y_i is the value of this function after adjustment. In the model, the objective function is the *E. coli* concentration in the effluent after UV inactivation; an influent *E. coli* concentration of 1.94×10^5 CFU/m^3, exposure time of 10 s, UV average absorbed energy density of 15.2 W/m^3, and k of 0.00593 under UVC irradiation (fitted from Section 3.1) were also adopted. Moreover, the value of p is 1.2 times of p_0. The sensitivity of the parameters of the model was analyzed, and the RSIs of t, Q, r, and S_L are listed in Table 4.

Effluent *E.coli* concentration N_{UV} was directly proportional to influent concentration N_0 with an RSI of 1. By contrast, negative relations existed between N_{UV} and exposure time t, light source strength per unit length S_L, and reactor radius r. Among the parameters tested, N_{UV} was the most sensitive to flow rate Q (*RSI*, 2.072), thereby indicating that high flow rate results in significantly low inactivation efficiency.

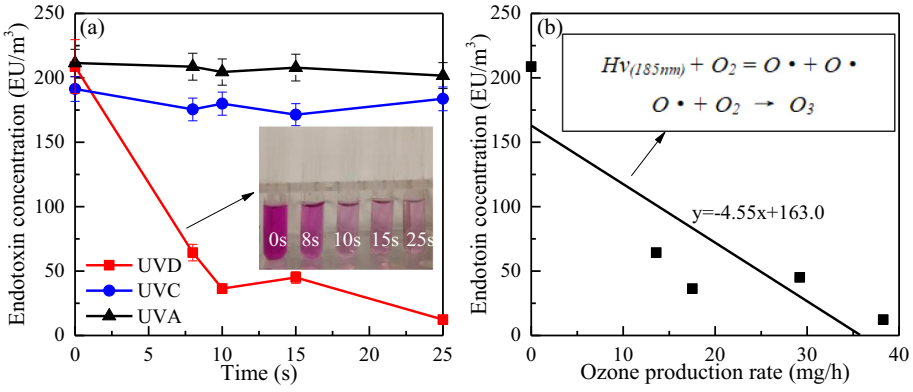

Fig. 5. (a) Removal of airborne endotoxin under different UV source. (b) Endotoxin concentration vs. ozone production rate under UVD.

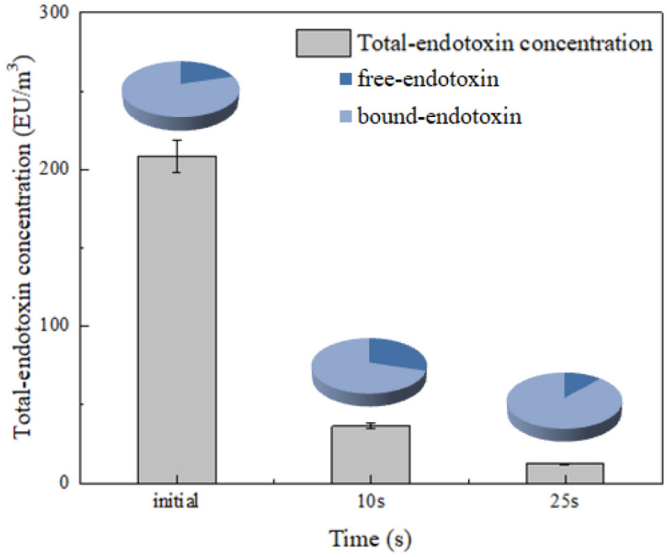

Fig. 6. Degradation of different type of endotoxin during UVD treatment.

3.3. Energy utilization during inactivation

Energy consumption (EC), a common index in the electrochemical oxidation field (Gurung et al., 2018; Wang et al., 2014), was used to measure the energy utilization efficiency of a process. In this study, only the energy consumed by UV lamps was taken into account while other consumption was not included. As discussed above, our model showed good agreement with the experimental data. To optimize airborne bacteria inactivation and improve economic efficiency, EC (Zhou et al., 2018) was adjusted and applied to evaluate energy utilization during UV inactivation process. Here, EC is defined as the average electrical energy consumed (power multiplied by time) required to inactivate 1 CFU of bacterium in 1 m^3 of air (Eq. 12). Thus a lower EC corresponds to a higher electrical energy utilization efficiency when inactivating 1 CFU of bacterium.

$$\mathrm{EC(J/CFU)} = \frac{P \cdot t}{V \cdot (N_0 - N)} \tag{12}$$

Fig. 4 illustrates changes in EC (log scale) as a function of UV dose and influent *E. coli* concentration after exposure to different UV sources. Cool colors (such as purple and blue) represent low EC values, while warm colors (such as red and orange) represent high values. A significant difference in EC between UVD and UVC was not found, although the latter was slightly higher than the former. The EC values obtained from the UVA treatment were remarkably higher than those obtained from the UVD and UVC treatments, corresponding to the different inactivation efficiencies observed in Section 3.1. Furthermore, low influent *E. coli* concentrations and high UV doses resulted in relatively higher EC values, thus suggesting that higher EC is required to achieve higher inactivation efficiency.

3.4. Changes in airborne endotoxins during inactivation

3.4.1. Endotoxin degradation and the corresponding mechanism

As a constituent of the Gram-negative bacterial cell membrane, endotoxins may be released during bacterial inactivation and bursting. Thus, measuring the change in endotoxin concentration from airborne microorganisms during UV treatment is necessary. The concentrations of airborne endotoxins were measured before and after UV treatment with different UV sources, and the results are shown in Fig. 5(a).

The total endotoxin concentration did not change significantly after treatment by UVA or UVC because the photo energy of UVA and UVC irradiation is too weak to break the molecular structure of endotoxins. UVA and UVC irradiation exerted no significant effect on the removal of endotoxins. However, the total-endotoxin concentration showed an obvious decrease with increasing exposure time under UVD treatment, possibly due to the generation of ozone. The change in endotoxin concentration with ozone production rate is shown in Fig. 5(b).

UVD irradiation is capable of sterilizing bioaerosols by generating ozone from oxygen in the air, as well as by damaging the DNA of microorganisms through irradiation (Eischeid et al., 2009). The ozone generation path is as follows:

$$Hv_{(185\ nm)} + O_2 = O + O$$

$$O + O_2 \rightarrow O_3$$

Ozone inactivates airborne bacteria by oxidizing their cell membrane. Besides DNA, the cellular structure of the microbes is destroyed, which increases the possibility of degrading endotoxins attached to the cell membrane. As ozone can oxidize endotoxins and decompose them into smaller molecules, removal of airborne endotoxins and the pathways of endotoxin degradation by ozone should be studied through further experiments.

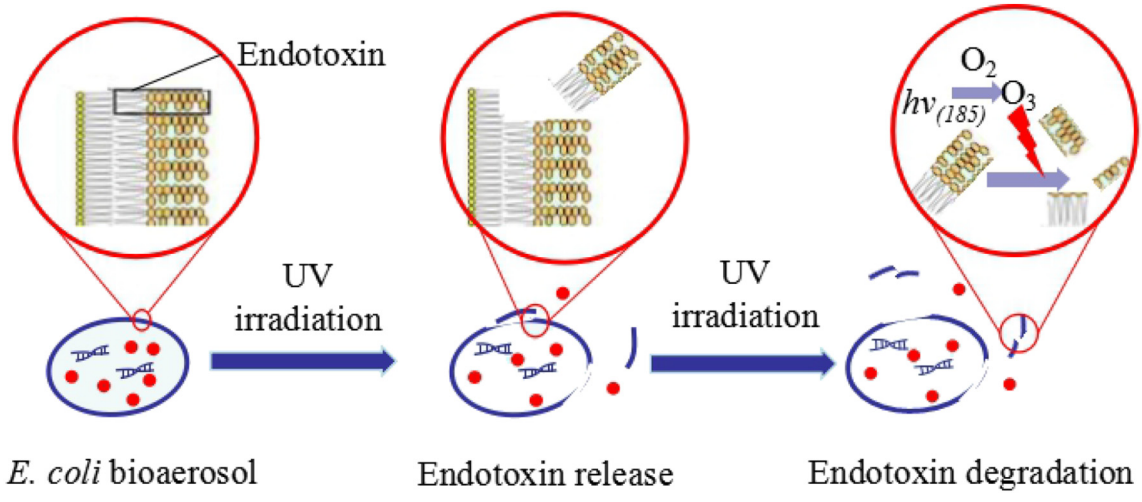

Fig. 7. Proposed degradation mechanism of endotoxin under UVD treatment.

3.4.2. Changes in free and bound endotoxins

The change in different types of endotoxins was further explored during UVD irradiation. Airborne endotoxins are present in the air in two main forms. The first corresponds to pure LPS molecules (free endotoxins). The second form corresponds to LPSs associated with other cell wall components or an intact bacterial cell (bound endotoxins) (Duquenne et al., 2013). Fig. 6 shows the change in the concentrations of total, free, and bound endotoxins with exposure time. Free endotoxins initially made up about 20% of the total endotoxin concentration. The concentrations of both free and bound endotoxins decreased gradually as exposure time increased, thereby indicating that UVD treatment has good ability to remove endotoxins regardless of type. The ratio of free endotoxins first increased and then decreased with time, indicating a possible release or transformation from bound to free endotoxins at the beginning of the UV irradiation process and subsequent degradation. A proposed degradation mechanism is shown in Fig. 7.

To the best of our knowledge, the degradation of airborne endotoxins has never been reported, and few scholars have conducted research on the degradation of waterborne endotoxins (Oh et al., 2014). Some oxidative processes employing free chlorine, ozone, plasma, and advanced oxidation processes (O_3/H_2O_2 and UV/H_2O_2) (Oh et al., 2014; Zhang et al., 2016) have been reported for waterborne endotoxin degradation. The present study is the first to report endotoxin degradation in an atmospheric environment. The results of this study may help provide new strategies to control airborne endotoxins and mitigate the environmental impacts of bioaerosols.

4. Conclusion

This study investigated and compared the inactivation performance of three UV sources (UVD, UVC, and UVA) toward aerosolized *E. coli* by modeling their inactivation efficiency, energy utilization, and endotoxin removal ability. Inactivation efficiency of 0.5, 2.2 and 3.1 logarithmic order was obtained at an exposure UV dose of 370 J/m^3 under UVA, UVC and UVD treatment, respectively. UVD and UVC were significantly more effective than UVA for inactivating bacteria. Modeling enabled prediction of inactivation efficiencies and analysis of the parameters that may affect inactivation constant *k*. Energy utilization efficiency was also analyzed by measuring E values. High EC was generally required in the case of relatively low influent *E. coli* concentrations and high UV doses, especially for the UVA inactivation process.

Changes in airborne endotoxin concentration during UV inactivation were measured in this work. Whereas UVC and UVA showed no effect on endotoxin degradation, both free and bound endotoxins could be removed by UVD treatment, which was attributed to the ozone generated by the UVD source during irradiation. The ratio of free endotoxins first increased then decreased with time, indicating a possible release or transformation from bound to free endotoxins during UV irradiation.

Acknowledgement

This study was supported by the National Natural Science Foundation of China (Grant No. 51678402).

Appendix A. Supplementary data

Supplementary data to this article can be found online at https://doi.org/10.1016/j.scitotenv.2018.11.266.

References

Akehata, T., Ito, K., Inokwa, A., 1976. Applications of the second law of thermodynamics to cryogenics - a review/energy. Trans. Jpn. Soc. Mech. Eng., B 34, 583–588.
Alfano, O.M., Romero, R.L., Cassano, A.E., 1986. Radiation field modeling in photoreactors-I. Homogeneous media. Chem. Eng. Sci. 41, 421–444.
Araud, E., Shisler, J.L., Nguyen, T.H., 2018. Inactivation mechanisms of human and animal rotaviruses by solar UVA and visible light. Environ. Sci. Technol. 52, 5682–5690.
Becker, P., 2001. History and progress in the accurate determination of the Avogadro constant. Rep. Prog. Phys. 64, 1945–2008.
Collins, H., Selleck, R., 1971. Problem in obtaining adequate sewage disinfection. JSAE. 97. ASCE, pp. 549–562.
Crittenden, J.C., Trussell, R.R., Hand, D.W., Howe, K.J., 2011. MWH's water treatment: principles and design. third edition. John Wiley & Sons, Inc, pp. 912–924.
Demonty, J., Grawe, J.D., 1982. Release of endotoxic lipopolysaccharide by sensitive strains of *Escherichia coli* submitted to the bactericidal action of human serum. Med. Microbiol. Immunol. 170, 265–277.
Dufour, N., Delattre, R., Ricard, J.D., Debarbieux, L., 2017. The lysis of pathogenic *Escherichia coli* by bacteriophages releases less endotoxin than by β-lactams. Clin. Infect. Dis. 64, 1582–1588.
Duquenne, P., Marchand, G., Duchaine, C., 2013. Measurement of endotoxins in bioaerosols at workplace: a critical review of literature and a standardization issue. Ann. Occup. Hyg. 57, 137–172.
Eischeid, A.C., Meyer, J.N., Linden, K.G., 2009. UV disinfection of adenoviruses: molecular indications of DNA damage efficiency. Appl. Environ. Microbiol. 75, 23–28.
Gergen, P.J., 2011. Understanding the economic burden of asthma. J. Allergy Clin. Immunol. 107, S445–S448.
Gibson, J., Drake, J., Karney, B., 2017. UV disinfection of wastewater and combined sewer overflows. Adv. Exp. Med. Biol. 996, 267.
Gurung, K., Ncibi, M.C., Shestakova, M., Sillanpaa, M., 2018. Removal of carbamazepine from MBR effluent by electrochemical oxidation (EO) using a Ti/Ta_2O_5-SnO_2 electrode. Appl. Catal. B Environ. 221, 329–338.
Inokawa, A., 1980. The exergy method of energy systems analysis. Trans. Jpn. Soc. Mech. Eng., B 38, 178–183.
Ishiguro, H., Yao, Y., Nakano, R., et al., 2013. Photocatalytic activity of Cu^{2+}/TiO_2-coated cordierite foam inactivates bacteriophages and *Legionella pneumophila*. Appl. Catal. B Environ. 129, 56–61.
Jacob, S.M., Dranoff, J.S., 1968. Design and analysis of perfectly mixed photochemical reactors. Chem. Eng. Prog. Symp. Ser. 64, 54–63.
Jensen, P.A., Lambert, L.A., Iademarco, M.F., Ridzon, R., 1994. Guidelines for preventing the transmission of Mycobacterium tuberculosis in health-care facilities, 1994. MMWR 43.RR-17, 1–141.
Kim, J., Jang, J., 2018. Inactivation of airborne viruses using vacuum ultraviolet photocatalysis for a flow-through indoor air purifier with short irradiation time. Aerosol Sci. Technol. 52, 557–566.
King, B., Kesavan, J., Sagripanti, J., 2011. Germicidal UV sensitivity of bacteria in aerosols and on contaminated surfaces. Aerosol Sci. Technol. 45, 645–653.
Koizumi, J., Yabe, I., Aiba, S., 1980. The exergy method of energy systems analysis. Trans. Jpn. Soc. Mech. Eng., B 38, 178–183.
Koller, L.R., 1952. Ultraviolet Radiation. John Wiley & Sons, New York, p. 8.
Kong, X., Wang, C., Ji, 2013. Analysis of microbial metabolic characteristics in mesophilic and thermophilic biofilters using Biolog plate technique. Chem. Eng. J. 230, 415–421.
Kowalski, W.J., William, P.B., 2000. Effective UVGI system design through improved modeling. ASHRAE Trans. 106, 4–15.
Liang, Y.D., Wu, Y., Sun, K., Chen, Q., Shen, F.X., Zhang, J., Yao, M.S., Zhu, T., Fang, J., 2012. Rapid inactivation of biological species in the air using atmospheric pressure nonthermal plasma. Environ. Sci. Technol. 46, 3360–3368.
Liu, H., Zhang, Z., Wen, N., Wang, C., 2018. Determination and risk assessment of airborne endotoxin concentrations in a university campus. J. Aerosol Sci. 115, 146–157.
Lytle, C.D., Sagripanti, J.L., 2005. Predicted inactivation of viruses of relevance to biodefense by solar radiation. J. Virol. 79, 14244–14252.
Mattsbybaltzer, I., Lindgren, K., Lindholm, B., Edebo, L., 1991. Endotoxin shedding by enterobacteria: free and cell-bound endotoxin differ in limulus activity. Infect. Immun. 59, 689–695.
Mendy, A., Cohn, R.D., Thorne, P.S., 2016. Endotoxin exposure, serum vitamin D, asthma and wheeze outcomes. Respir. Med. 114, 61–68.
Mortensen, N.A., Xiao, S., 2007. Slow-light enhancement of Beer-Lambert-Bouguer absorption. Appl. Phys. Lett. 90, 374.
Nilsson, S., Merritt, A.S., Bellander, T., 2011. Endotoxins in urban air in Stockholm, Sweden. Atmos. Environ. 45, 266–270.
Noakes, C.J., Khan, M.A.I., Gilkeson, C.A., 2015. Modeling infection risk and energy use of upper-room ultraviolet germicidal irradiation systems in multi-room environments. Sci. Technol. Built Environ. 21, 99–111.
Oh, B.T., Seo, Y.S., Sudhakar, D., Choe, J.H., Lee, S.M., Park, Y.J., Cho, M., 2014. Oxidative degradation of endotoxin by advanced oxidation process (O_3/H_2O_2 & UV/H_2O_2). J. Hazard. Mater. 279, 105–110.
Oldenburg, M., Latza, U., Baur, X., 2007. Exposure–response relationship between endotoxin exposure and lung function impairment in cotton textile workers. Int. Arch. Occup. Environ. Health 80, 388–395.
Ono, R., Yonetamari, K., Tokumitsu, Y., Yonemori, S., Yasuda, H., Mizuno, A., 2016. Inactivation of Bacillus atrophaeus by OH radicals. J. Phys. D. Appl. Phys. 49.
Otake, T., Tone, S., Higuchi, K., Nakao, K., 1983. Applicability of effective absorption coefficient. Int. Chem. Eng. 23, 288–297.
Reiman, M., Uitti, J., 2000. Exposure to microbes, endotoxins and total dust in cigarette and cigar manufacturing: an evaluation of health hazards. Ann. Occup. Hyg. 44, 467–473.
Ryan, K., McCabe, K., Clements, N., Hernandez, M., Miller, S.L., 2010. Inactivation of airborne microorganisms using novel ultraviolet radiation sources in reflective flow-through control devices. Aerosol Sci. Technol. 44, 541–550.
Sagripanti, J.L., Levy, A., Robertson, J., Merritt, A., Inglis, T.J.J., 2009. Inactivation of virulent *Burkholderia pseudomallei* by sunlight. Photochem. Photobiol. 85, 978–986.
Sreeja, S., Shetty, V.K., 2016. Microbial disinfection of water with endotoxin degradation by photocatalysis using Ag@TiO2 core shell nanoparticles. Environ. Sci. Pollut. Res. Int. 23 (181541-18154).

Takashima, H., Miyakawa, Y., Kanno, Y., 2007. Microwave sterilization with metal thin film coated catalyst in liquid phase. Mater. Sci. Eng. C Mater. Biol. Appl. 27, 898–903.
Tang, W.L., Guo, Z.Y., 2005. Influence of ultraviolet radiation on calf thymus DNA studied by Raman spectroscopy. In: Chance, B., Chen, M., Chiou, A., Luo, Q. (Eds.), Proceedings of the Society of Photo-optical Instrumentation Ginerrs. SPIE, pp. 384–395.
Walker, C.M., Ko, G., 2007. Effect of ultraviolet germicidal irradiation on viral aerosols. Environ. Sci. Technol. 41, 5460.
Wang, C., Huang, Y.K., Zhao, Q., Ji, M., 2014. Treatment of secondary effluent using a three-dimensional electrode system: COD removal, biotoxicity assessment, and disinfection effects. Chem. Eng. J. 243, 1–6.
Wang, D., Zhu, B., He, X., et al., 2018. Iron oxide nanowires based filter for inactivation of airborne bacteria. Environ. Sci. Nano. 5, 1096–1106.
Wen, N., Liu, H., Fu, Y., Wang, 2017. Optimization and influence mechanism of sampling and analysis of airborne endotoxin based on limulus amebocyte lysate assay. Aerosol Air Qual. Res. 17, 1000–1010.
Xu, P., Peccia, J., Fabian, P., et al., 2003. Efficacy of ultraviolet germicidal irradiation of upper-room air in inactivating airborne bacterial spores and mycobacteria in full-scale studies. Atmos. Environ. 37, 405–419.
Xu, P., Kujundzic, E., Peccia, J., Schafer, M.P., Moss, G., Hernandez, M., Miller, S.L., 2005. Impact of environmental factors on efficacy of upper-room air ultraviolet germicidal irradiation for inactivating airborne mycobacteria. Environ. Sci. Technol. 39, 9656–9664.
Yokota, T., Iwano, T., Saito, A.T., Tadaki, T., 1981. Photochlorination of toluene in a bubble column photochemical reactor. Int. Chem. Eng. 7, 164–170.
Zhang, Q., Damit, B., Welch, J., Park, H., 2010. Microwave assisted nanofibrous air filtration for disinfection of bioaerosols. J. Aerosol Sci. 41, 880–888.
Zhang, C., Fang, Z., Liu, W., Tian, F., Bai, M., 2016. Rapid removal of bacterial endotoxin and natural organic matter in water by dielectric barrier discharge plasma: efficiency and toxicity assessment. J. Hazard. Mater. 318, 15–23.
Zhao, Y., Aarnink, A.J., Xin, H., 2014. Inactivation of airborne *Enterococcus faecalis* and infectious bursal disease virus using a pilot-scale ultraviolet photocatalytic oxidation scrubber. J. Air Waste Manage. Assoc. 64, 38–46.
Zhou, S., Yu, Y., Zhang, W., Meng, X., Luo, J., Deng, L., Shi, Z., Crittenden, J., 2018. Oxidation of microcystin-LR via activation of peroxymonosulfate using ascorbic acid: kinetic modeling and toxicity assessment. Environ. Sci. Technol. 52, 4305–4312.